Toward the Origin of Long-Period Long-Duration Seismic Events during Hydraulic Fracturing Treatment: A Case Study in the Shale Play of Sichuan Basin, China

by Haichao Chen, Fenglin Niu, Youcai Tang, and Kai Tao

ABSTRACT

Long-period long-duration (LPLD) seismic events have been recently observed over several unconventional reservoirs, and are postulated to play a significant role in accommodating deformation within the stimulation zone. However, the origin of LPLD events is still under debate. In this study, we present observations of tremor-like events during the multistage hydraulic fracturing treatment of a pilot horizontal well within the Weiyuan Shale play in southwestern Sichuan basin, China. These tremor-like signals recorded by the deep downhole monitoring array (15 Hz geophones) resemble the previously reported LPLD examples in terms of both duration and frequency content. In this particular case, with the concurrent records from the surface broadband array, we however confirm that these signals are located well outside the treatment area, and most probably originate from regional earthquakes that occurred during the treatment course within 250 km radius of the treatment well, instead of local sources directly related to the hydraulic stimulation. This study implies that the attenuated signals of regional seismicity may constitute a particularly deceptive pitfall for identifying and misinterpreting LPLD events during hydraulic fracturing, especially in seismically active regions. Our results also highlight the importance of surface broadband array in monitoring hydraulic fracturing activities.

Electronic Supplement: Seismograms, spectrograms, and map of low-frequency stacked energy.

INTRODUCTION

Long-period long-duration (LPLD) seismic events are low-frequency tremor-like signals that have been recently observed during hydraulic fracturing treatments over unconventional reservoirs (Das and Zoback, 2013a,b; Eaton *et al.*, 2013). These events typically persist up to one minute without clear impulsive arrivals and are rich in relatively low-frequency energy (10–80 Hz). Owing to their similar signal features with tectonic tremors in the subduction zone, LPLD events are also commonly interpreted in terms of fluid-driven process. In particular, they are presumed to be associated with slowly cascading rupture process along pre-existing fractures or faults that are unfavorably oriented for reactivation with respect to the present-day stress field, due to high fluid pressure or high clay content (Zoback *et al.*, 2012; Das and Zoback, 2013b; Hu *et al.*, 2017). In addition, Kanamori and Hauksson (1992) documented a clear example of a slow earthquake near Santa Maria, California, on 31 January 1991, which occurred a few hours after hydraulic fracturing operation and was likely associated with fluid injection. Tary, van der Bann, and Eaton (2014) and Tary, van der Bann, Sutherland, *et al.* (2014) also reported another type of LPLD events related to hydraulic fracturing, which are interpreted as resonance of fluid-filled cracks. Because of their long duration, the cumulative energy released by LPLD events is significantly higher than that of commonly observed microearthquakes (Das and Zoback, 2013a). As a consequence, LPLD events are postulated to play a crucial or even dominant role in accommodating deformation within the stimulation zone and contribute substantially to the permeability enhancement in extremely tight reservoirs.

However, the origin and nature of LPLD events remain controversial. First, in contrast to microseismic events that are generally inherent to hydraulic stimulation, LPLD events are not widespread over unconventional reservoirs and only documented in a handful of shale gas plays, including Barnett Shale in Texas (Das and Zoback, 2013a), Marcellus Shale in Green County, Pennsylvania (Kumar *et al.*, 2017), Eagle Ford Shale in northeast Mexico (Hu *et al.*, 2017). Moreover, the occurrence of these tremor-like events appear to be sporadic, without obvious temporal correlation with pumping activities, neither with the occurrence of microseismic events. Recently,

doi: 10.1785/0220170270

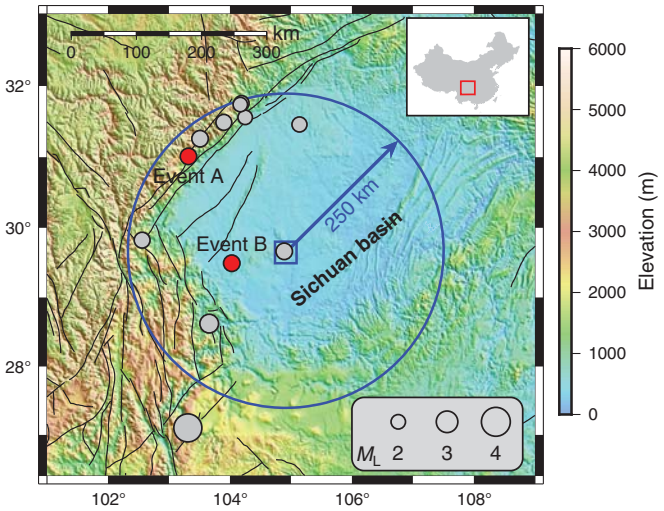

▲ **Figure 1.** The inset map shows the location of the study area in China, and the main map presents the spatial distribution of the regional earthquakes (gray circles) that occurred during the hydraulic stimulation and corresponds to the 12 observed long-period long-duration (LPLD) events in this study, based on the national earthquake catalog maintained by China Earthquake Data Center (see Data and Resources). The two typical LPLD events (events A and B) used in this study are marked with red circles. The open square denotes the location of the treatment well. The faults in the study area are marked with black lines.

Caffagni *et al.* (2015) suggested that regional seismicity recorded by 15 Hz downhole geophones share the same signal features of LPLD events in terms of both frequency content (< 100 Hz) and duration (~1 min), and thus may act as a potential pitfall for identifying LPLD events. With the wide spatial coverage of USArray, Zecevic *et al.* (2016) located all of the LPLD events documented in the Barnett Data 2 by Das and Zoback (2013a) well outside the treatment well area, and thereby concluded that the LPLD events are probably weakened records of small earthquakes that lie beneath the detection threshold of the regional network, rather than locally sourced events related to the hydraulic stimulation process.

Typically, LPLD events are recorded by a linear downhole geophone array. It is noted that we still refer to the tremor-like signals during hydraulic stimulation as LPLD events. The locations of LPLD events are usually poorly constrained, partly ascribed to lack of clear phase arrivals and limited aperture of the monitoring array (Das and Zoback, 2013b). Thus, most previous studies generally focused on the waveform characteristics of LPLD events. Besides, the records from bandlimited geophones only provide a glimpse into LPLD events. Although the temporal coincidence suggests that the LPLD events might originate from weakened signals of regional seismicity, it is still difficult to distinguish LPLD events from the regional earthquakes. Hence, the nature and origin of LPLD events remain to be explored.

In this study, we report a case study of LPLD events during the hydraulic fracturing treatment of a pilot horizontal well within the Weiyuan Shale play in southwestern Sichuan basin, China (Fig. 1). The treatment was monitored using a deliberately designed hybrid monitoring array, which consisted of a deep downhole geophone array and a temporary surface broadband array. A total of 12 LPLD seismic events were identified during the whole treatment course. We first give an overview of the signal characteristics of the observed LPLD events, which are characterized by low frequencies of 5–40 Hz and long durations of 30–60 s, similar to the previously reported LPLD examples in other regions. Then, we display beamforming analysis and source scanning results using the LPLD records from the surface broadband array, which provide unambiguous evidence that all the LPLD events correspond to regional earthquakes within 250 km of the treatment well.

LPLD EVENTS

Monitoring Array

Weiyuan area has been one of the major shale gas reservoirs in China. The complex tectonic history in this area resulted in very complex structures with extensive folding and faulting (Liang *et al.*, 2015). Multiscale natural fractures and strike-slip faults are commonly observed with strike directions predominantly in the N40°–60°E range (Chen *et al.*, 2017). A massive multistage hydraulic fracturing treatment was performed during the period from 28 October to 10 November 2014 to enhance the production of a pilot horizontal well in the Weiyuan Shale play. There are 19 treatment stages along the 1900-m-long horizontal section of the treatment well (Fig. 2a), with each treatment stage lasting ~3 hrs. A hybrid seismic array, consisting of a deep downhole geophone array and a surface broadband array, was deployed to continuously monitor the fracturing process over the whole course of the treatment. The downhole array consisted of 20 levels of triaxial 15 Hz geophones, which was deployed in a nearby vertical monitoring well at a depth from 2120 to 2405 m, with a sensor spacing of 15 m and a sampling rate of 2000 Hz (Fig. 2a). The broadband array was composed of 22 temporary broadband seismic stations, forming two rings with aperture ~1 and ~3 km, respectively (Fig. 2b). Güralp CMG-3T and CMG-40T seismometers were used, which have a flat velocity response between 0.03 and 50 Hz, with a very high sensitivity of 2400 m/(V/s).

Signal Features of LPLD Events

Motivated by the recently reported class of LPLD events, we visually inspected the spectrogram of the 15-day-long continuous downhole dataset to search for similar LPLD events. A total of 12 well-recorded long-duration tremor events were identified during the whole treatment course, among which 5 events occurred during the injection period and 7 events during the postinjection period, showing no obvious temporal correlation with the injection activities. There were no LPLD events observed before the pumping, because the downhole records only started shortly before the onset of injection. Compared to typical microseismic events (less than 1 s), these signals feature long duration ranging from 30 to 60 s, without

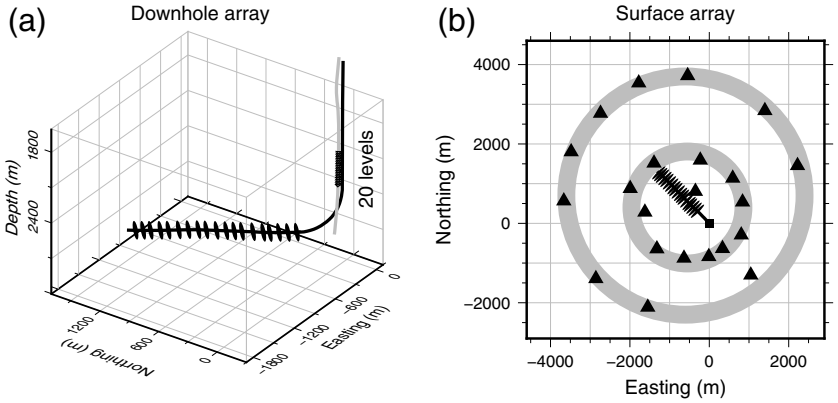

▲ **Figure 2.** (a) The 3D view of the downhole monitoring array. The wellhead of the monitoring well (gray line) is laterally separated from that of the treatment well (black line) by about 60 m. The downhole monitoring array consists of 20 levels of triaxial 15 Hz geophones (black triangles) at a depth from 2120 to 2405 m with sensor spacing of 15 m, about 300 m above the perforation shots of the treatment stages (black ellipsoids). (b) Map view of the surface monitoring array, which was composed of 22 temporary broadband stations (black triangles), forming two rings with aperture ~1 and ~3 km, respectively (gray circles). The solid black square denotes the wellhead of the treatment well. The perforation shots of 19 treatment stages along the 1900-m-long horizontal section of the treatment well (black line) are marked by solid black ellipsoids.

impulsive phase arrivals. Figure 3a,b presents the filtered vertical seismograms (0.5–100 Hz) of two typical tremor-like events recorded by the deepest geophone, as well as the corresponding spectrograms. In addition to the relatively long duration, the waveforms are dominated by frequencies in the 5–40 Hz range, slightly lower than the LPLD events in Barnett Shale (Das and Zoback, 2013a). There is a persistent signal at ~33 Hz in the spectrograms of both events, which is likely to be local resonances due to interactions between the injected fluid and the wellbore (Tary, van der Bann, and Eaton, 2014). Besides, it is obvious that the event in Figure 3a features longer duration and lower frequency content than the one in Figure 3b. Hereafter, we refer to these two typical events as events A and B, respectively. Figure 4a displays the vertical waveforms of event A recorded by several downhole receiver levels. Interestingly, the waveforms show a low-frequency and low-amplitude precursor, followed by a relatively high-amplitude main event. The enlargement of a short time window within the precursor (Fig. 4b) and the main event (Fig. 4c) shows obvious moveout across the downhole array, with apparent velocity of 6.88 and 3.75 km/s, respectively. This implies that the precursor signal travels at compressional wavespeed, whereas the main event propagates at shear wavespeed. Das and Zoback (2013a) also reported discrete phases of LPLD events with similar apparent velocities, which were subsequently used to estimate the incidence angles of the signals. Generally, the LPLD events, when recorded by the downhole geophones, are remarkably similar to the previously documented ones in terms of both duration and frequency content.

Because the resonance frequency of the typical downhole geophone is 15 Hz, useful information down to a few Hz is likely to go unnoticed because of limited bandwidth. Fortunately, in this study, these tremor-like signals were also concurrently recorded by the surface broadband array. Figure 3c,d shows the vertical seismograms of events A and B recorded by a three-component (3C) broadband station located near the wellhead of the treatment well, as well as the corresponding spectrograms. The spectrograms of the two horizontal seismograms of event A are also exhibited in Ⓔ Figure S1 (available in the electronic supplement to this article). It is obvious that there is abundant low-frequency energy down to 1 Hz, which was not recorded by the downhole geophone array. Moreover, impulsive seismic phases (both *P* and *S* waves) are clearly observed in the band-pass-filtered 3C waveforms (0.5–2 Hz, see Ⓔ Fig. S2).

EVIDENCE OF REGIONAL EARTHQUAKES

Regional Earthquake Catalog

Based on the national earthquake catalog maintained by China Earthquake Data Center, there are tens of earthquakes within 250 km radius of the treatment well during the timeframe of the reservoir stimulation operation, which have known locations, local magnitudes, and origin times. Similar to Caffagni *et al.* (2015), we first carefully checked the observed LPLD events against the national earthquake catalog and found that there is temporal overlap (within 10 s) between the arrival time of each individual LPLD event and the expected arrival time of one of these regional earthquakes, using the simple IASP91 reference velocity model. These regional earthquakes, which correspond to the LPLD seismic events, are shown in Figure 1 and also listed in Table 1. Particularly, both events A and B in Figure 3 correspond to regional earthquakes of M_L 2.3 (red circles in Fig. 1; events 8 and 9 in Table 1), with epicentral distance from the treatment well of 87.4 and 215.5 km, respectively. The fracking operation also induced one seismic event with local magnitude greater than 2. Given that the adjacent area is quite seismically active, the temporal coincidence strongly indicates that the observed sporadic LPLD seismic events probably originate from the regional tectonic events.

Beamforming and SSA Analysis

In this section, we first performed beamforming analysis to determine the source direction of the observed LPLD events. We applied plane-wave frequency domain beamforming to the vertical records from the surface broadband array, generally following the methodology of Gerstoft and Tanimoto (2007). We formed beams and determined the azimuth and slowness of the waves propagating through the array as a function of

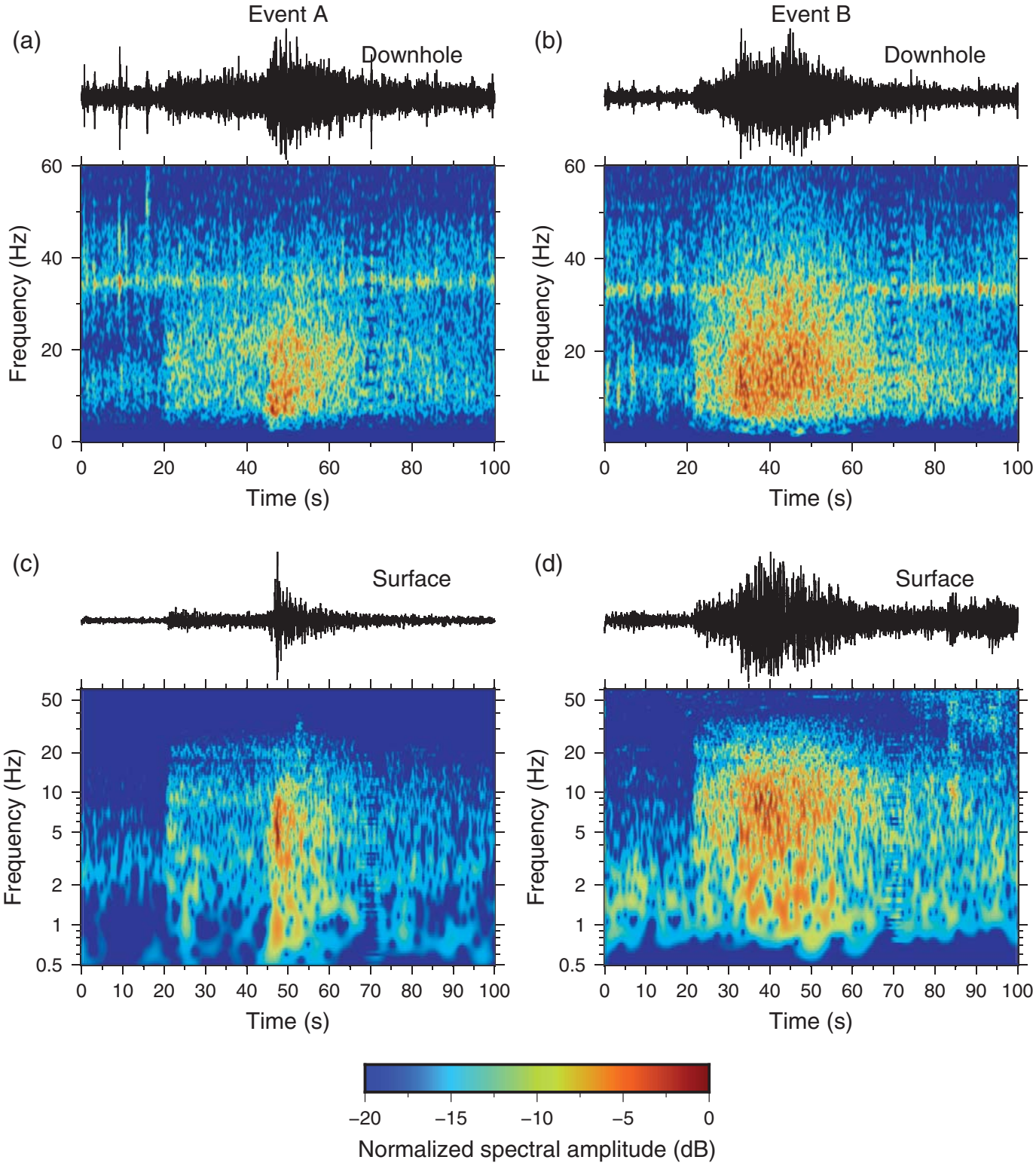

▲ **Figure 3.** The filtered vertical seismograms (0.5–100 Hz) and the corresponding spectrograms of two typical tremor-like events (events A and B) recorded by (a,b) the deepest geophone and (c,d) a surface broadband station located near the wellhead of the treatment well. Note that the normalized spectral amplitude of the spectrogram is plotted on a logarithmic scale.

frequency. As an example, Figure 5a exhibits the beamform output of event A at a relatively low-frequency band (1–3 Hz). There are two distinct signals in the direction of ~316 (white crosses), in agreement with the back azimuth of the corresponding regional earthquake (black dashed line). The two signals have apparent velocity of 6.1 and 3.3 km/s, respectively, which

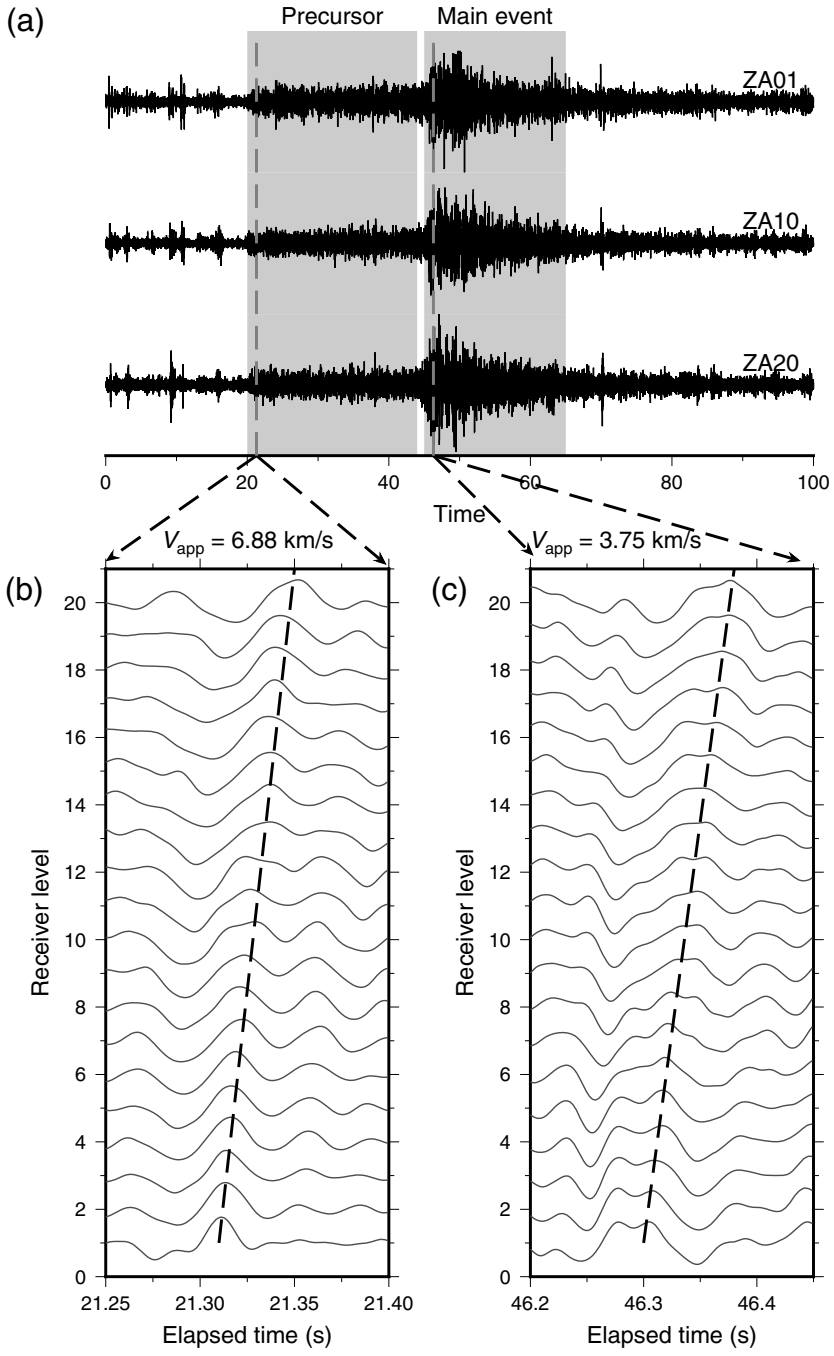

▲ **Figure 4.** (a) The vertical waveforms of event A recorded by several downhole receiver levels, which shows a low-frequency and low-amplitude precursor (left gray shadow), followed by a relatively high-amplitude main event (right gray shadow). The enlargement of a short time window within (b) the precursor and (c) the main event show obvious moveout across the downhole array, with apparent velocity of 6.88 and 3.75 km/s, respectively.

possibly correspond to the precursor (*P* wave) and main event (*S* wave) in Figure 4 and Ⓔ Figure S2. As expected, the beamforming output in the low-frequency band clearly indicates that the energy comes from outside the treatment region, and originates dominantly from the back-azimuthal direction of the corresponding regional earthquake.

Because of the limited downhole array geometry, Das and Zoback (2013b) can only estimate the arrival angle of the LPLD events with respect to the array from the moveout across the array, and then choose the most likely location based on the site of the current treatment stage. One of the most commonly used methods for locating tremor-like signals is the source scanning algorithm (SSA; Kao and Shan, 2004), which has also been modified to detect and locate microseismic events induced by hydraulic stimulation (Drew *et al.*, 2013). In this study, we adapted the SSA to search the potential location of the observed LPLD events within a restricted region in the neighborhood of the treatment well, using vertical records from the surface broadband array. We briefly outline the procedures here. First, we bandpass filter the waveform within the frequency band of interest and calculate the waveform envelope. Then, we set up a meshed 3D region around the treatment well, and stack all the amplitude envelopes over the monitoring array along the differential moveout of each grid node within the search volume, to obtain the 3D stacked energy image. Ⓔ Figure S3 displays the map view of the contour map of the stacked energy at a depth of ~2700 m for event B in a relatively low-frequency band (0.5–2 Hz). The stacked energy appears to be dominated by a coherent source. The grid node of maximum energy is located on the southwestern boundary of the searching volume, consistent with the back azimuth of the corresponding region earthquake (gray arrows), implying that the actual source is located well outside the searching volume. Conversely, in the case of high-frequency range (10–30 Hz), the stacked energy is dominated by highly diffusive wavefield (Fig. 5b), probably originating from several scattered sources. The stacked energy image of the other LPLD events generally exhibit similar pattern. The spatial distribution of the microseismicity is also shown for reference (magenta circles). In spite of nearly identical treatment strategy across all the 19 treatment stages, the seismic response is highly variable (Chen *et al.*, 2017), with most microseismic events located in several clusters around both the heel and toe regions (red ellipsoids in Fig. 5b). It appears that these scattered energy patches are roughly coincident with the clustered distribution of microseismicity.

DISCUSSION

The Origin of LPLD Events

When recorded by typical 15 Hz downhole geophones, the observed LPLD events are remarkably similar to previously

Table 1
Catalog of Regional Earthquakes That Occurred During the Hydraulic Stimulation and Correspond to the 12 Observed Long-Period Long-Duration (LPLD) Events in This Study

Event ID	Origin time (UTC) (yyyy/mm/dd hh:mm:ss)	LPLD Arrival Time (UTC) (yyyy/mm/dd hh:mm:ss)	Longitude (E)	Latitude (N)	Depth (km)	M_L	Distance (km)
01	2014/10/29 10:32:03	2014/10/29 10:32:32	103.66	28.62	8	2.6	166.6
02	2014/11/02 15:44:13	2014/11/02 15:44:13	104.89	29.66	15	2.3	3.0
03	2014/11/02 17:12:59	2014/11/02 17:13:49	103.31	27.10	10	3.9	322.7
04	2014/11/05 01:40:57	2014/11/05 01:41:35	103.51	31.26	18	2.3	224.2
05	2014/11/05 10:40:44	2014/11/05 10:41:19	104.25	31.56	6	2.0	221.7
06	2014/11/05 11:18:09	2014/11/05 11:18:43	105.14	31.46	18	2.1	202.4
07	2014/11/06 03:18:14	2014/11/06 03:18:49	103.90	31.49	20	2.2	226.6
08	2014/11/06 15:26:50	2014/11/06 15:27:10	104.03	29.49	7	2.3	87.4
09	2014/11/07 03:03:19	2014/11/07 03:03:59	103.32	31.01	19	2.3	215.5
10	2014/11/07 22:28:21	2014/11/07 22:28:57	102.56	29.82	25	2.2	228.6
11	2014/11/09 10:39:13	2014/11/09 10:39:55	104.19	31.76	5	2.1	244.6
12	2014/11/09 11:00:26	2014/11/09 11:01:05	104.17	31.74	11	2.0	243.0

The arrival time of the corresponding LPLD event on a broadband station near the wellhead of the treatment well is also given for reference.

reported LPLD examples in terms of duration, frequency content, and waveform characteristics (Das and Zoback, 2013a,b; Kumar *et al.*, 2017). Hu *et al.* (2017) claimed that their LPLD events are different from previously described LPLD events by virtue of frequency spectra, which have peaks at several isolated frequencies. This argument is not so convincing because their spectral amplitude is presented on a linear scale, instead of a logarithmic scale. After checking the LPLD events against the national earthquake catalog, we found that the LPLD events are temporally coincident with the regional earthquakes at distance within 250 km radius of the treatment well. With the concurrent records from the surface broadband array, we further provide compelling evidence that these observed LPLD events located well outside the treatment region, and most probably originate from regional seismicity, instead of locally source events directly related to the induced reservoir deformation associated with the hydraulic stimulation. The weakened signals of regional earthquakes are characterized by complex waveform, due to strong scattering from crustal heterogeneities along the source–receiver path. Therefore, the partially overlapped coda of *P* and *S* waves might lead to a continuous long-duration signal, especially when recorded by a 15-Hz downhole geophone. Besides, the waveforms of regional earthquakes may be different, depending on the epicentral distance with respect to the treatment well (Fig. 3a,b).

It is very appealing that LPLD events might accommodate most of the deformation within the stimulation zone, and thereby, imaging this type of LPLD events can potentially map fluid flow and tensile fracture development during hydraulic fracturing (e.g., Hu *et al.*, 2017). Moreover, laboratory frictional experiments of shale samples under *in situ* pressure and temperature indicate that slow slip along pre-existing weak planes may exist within clay-bearing sedimentary rock (Zoback *et al.*, 2012; Kohli and Zoback, 2013; Bonnelye *et al.*, 2017). However, it should be kept in mind that LPLD events do not universally exist in response to hydraulic stimulation, and are only observed in a handful of shale gas plays. Although it is not clear whether the previously documented LPLD events also originate from regional seismicity, it is undoubted that the attenuated signals of regional earthquakes could be easily mistaken as being slow-slip events induced by the fracturing treatment and thus act as a particularly deceptive pitfall for misinterpretation of LPLD events during hydraulic fracturing, especially in seismically active regions (Caffagni *et al.*, 2015). Moreover, anthropogenic activities may also generate similar LPLD signals. For instance, Li *et al.* (2017) recently revealed that the long-duration tremor-like signals recorded during the Oklahoma wavefield experiment are most likely originating from nearby trains. It would be prudent to understand the origin of the observed LPLD events before interpreting LPLD events as being related to reservoir deformation process, especially when downhole geophone array is the only viable monitoring configuration.

It would be important to check the identified LPLD events against a regional earthquake catalog to enable discrimination based on timing to avoid misinterpretation of LPLD events. Nevertheless, it is possible that regional earthquakes lie below the detection threshold of permanent regional seismic network, and thus are missing from the regional earthquake catalog. In this scenario, independent seismic dataset acquired from surface monitoring array may play a vital role in distinguishing LPLD events related to hydraulic fracturing from weakened signals of regional earthquakes (e.g., Eaton *et al.*, 2013). Hence, we suggest install a few broadband seismic stations, as a useful complement to the downhole array, to monitoring future hydraulic fracturing activities. Because the

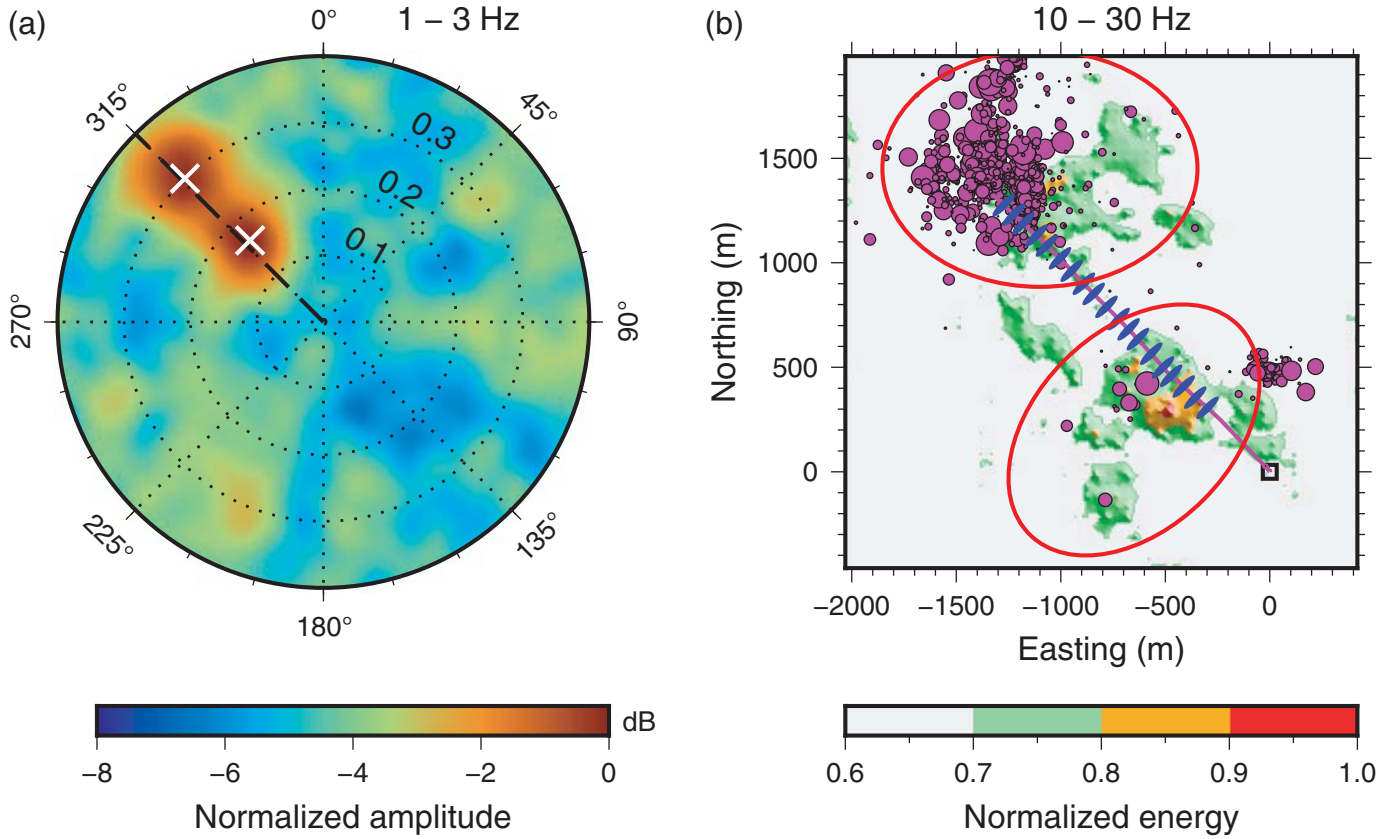

▲ **Figure 5.** (a) Beamform output of event A in the 1–3 Hz frequency band, using the vertical records from the surface broadband array. The black dashed line marks the back azimuth of the corresponding regional earthquake with respect to the treatment well. The two distinct signals at azimuth of ~316 (white crosses) have apparent velocity of 6.1 and 3.3 km/s, respectively. Note that the amplitude has been normalized by the maximum beamforming energy and are presented on a logarithmic scale. (b) Map view of the contour maps of the stacked energy at a depth of ~2700 m for event B in the 10–30 Hz frequency range. Note that the energy has been normalized by the maximum stacked energy and we only plot the region within 70% of the maximum stacked energy for sake of clarity. The well trajectory of the horizontal well (solid pink line) and the perforation shots (solid blue ellipsoids) are displayed for reference. The spatial distribution of the microseismicity (magenta circles) is also shown for comparison. The two open red ellipsoids mark the regions that are possibly of high natural fracture density.

resonance frequency of broadband seismometers is far below 1 Hz, they can avoid magnitude saturation. More importantly, they may enable us to determine the propagation direction of the low-frequency signals and thereby discriminate the regional earthquakes from potential true LPLD events. Furthermore, they can record the earthquake signals before the onset of injection and allow us to evaluate the background seismicity level in the target area. In this case study, the surface broadband array was deployed about one week before pumping began. Similar LPLD signals were also recorded before the injection, which were obviously not related to the pumping activities.

Scattering of High-Frequency Energy

Apparently, these attenuated records of regional earthquakes are not physically related to the stimulation process. Yet, it is interesting that the high-frequency energy patches are spatially coincident with the clustered distribution of microseismicity (Fig. 5b). Microseismic events are typically caused by brittle failure of pre-existing fractures. Consequently, the spatial clustering of microseismicity is probably strongly controlled by the pre-existing natural faults or fractures (Chen *et al.*, 2017). Thus, it is reasonable to speculate that the region with high natural fracture density may act as strong acoustic energy scatters (Zecevic *et al.*, 2016), which can generate a weak secondary wavefield that will be present in the recordings, when regional earthquakes illuminate the target reservoir. As a result, these energy patches are likely to be regarded as the source locations of the LPLD events, if searching the locations of LPLD events within a restricted volume by maximizing the stacked energy. For instance, Das and Zoback (2013b) located a subset of 10 large LPLD events in a cluster within a limited region of the reservoir, regardless of the stage that was being injected. On one hand, it may lead to the artifact that the LPLD events and the microseismicity share a common source. On the other hand, this also suggests that the scattered signals from regional seismicity can give some clues to the scattering properties of the target formation.

CONCLUSION

A total of 12 tremor-like seismic events were observed during the hydraulic fracturing treatment of a pilot horizontal well in the Weiyuan Shale play. We show that these LPLD events, when recorded by typical 15 Hz downhole geophones, are notably similar to previously reported LPLD examples in terms of duration, frequency content, and waveform characteristics. With the concurrent records from the surface broadband array, we however provide compelling evidence that these LPLD events most probably originate from regional earthquakes within 250 km radius of the treatment well. In addition to the temporal coincidence, the beamforming and source scanning analysis show that the propagation directions of these signals are consistent with the back azimuth of their corresponding earthquakes, which strongly indicates that these tremor-like signals are weakened signals of the regional seismicity, rather than local slow-slip events directly related to fluid presence and migration during hydraulic stimulation. This case study implies that the attenuated signals of regional seismicity may constitute a particularly deceptive pitfall for identifying and misinterpreting LPLD events during hydraulic fracturing, especially in seismically active regions. Moreover, the region of high natural fracture density may act as strong acoustic energy scatterers, which can generate a high-frequency secondary wavefield and thus potentially give some clues to the scattering properties of the target formation. This study also highlights the importance of surface broadband array in monitoring hydraulic fracturing operations.

DATA AND RESOURCES

The China Earthquake Data Center was searched using data.earthquake.cn (last accessed September 2017). All the plots were made using the Generic Mapping Tools v.5.3.1 (http://gmt.soest.hawaii.edu, last accessed February 2017; Wessel *et al.*, 2013). The waveforms used in this study were collected as part of the hydraulic fracturing monitoring experiment in Weiyuan Shale play. Data are available from the corresponding author upon request.

ACKNOWLEDGMENTS

The authors thank Sichuan Geophysical Company of China National Petroleum Company (CNPC) for providing the field dataset and permission to present this work, and Editor-in-Chief Zhigang Peng and two anonymous reviewers for their helpful comments. This work was jointly supported by the National Basic Research Program of China (973 Program, Number 2015CB250903), the National Natural Science Foundation of China (Numbers 41604043 and 41630209), and the Science Foundation of China University of Petroleum, Beijing (Numbers 2462014YJRC045 and 2462015YQ1203).

REFERENCES

Bonnelye, A., A. Schubnel, C. David, P. Henry, Y. Guglielmi, C. Gout, A. L. Fauchille, and P. Dick (2017). Strength anisotropy of shales deformed under uppermost crustal conditions, *J. Geophys. Res.* **122,** 110–129, doi: 10.1002/2016JB013040.

Caffagni, E., D. Eaton, M. van der Baan, and J. P. Jones (2015). Regional seismicity: A potential pitfall for identification of long-period long-duration events, *Geophysics* **80,** no. 1, A1–A5, doi: 10.1190/GEO2014-0382.1.

Chen, H. C., X. Meng, F. L. Niu, Y. C. Tang, C. Yin, and F. Wu (2017). Microseismic monitoring of stimulating shale gas reservoir in SW China: 2. Spatial clustering controlled by the pre-existing faults and fractures, *J. Geophys. Res.*, doi: 10.1002/2017JB014491 (in press).

Das, I., and M. D. Zoback (2013a). Long-period, long-duration seismic events during hydraulic stimulation of shale and tight-gas reservoirs —Part 1: Waveform characteristics, *Geophysics* **78,** no. 6, KS97–KS108, doi: 10.1190/GEO2013-0164.1.

Das, I., and M. D. Zoback (2013b). Long-period, long-duration seismic events during hydraulic stimulation of shale and tight-gas reservoirs —Part 2: Location and mechanisms, *Geophysics* **78,** no. 6, KS109–KS117, doi: 10.1190/GEO2013-0165.1.

Drew, J., R. S. White, F. Tilmann, and J. Tarasewicz (2013). Coalescence microseismic mapping, *Geophys. J. Int.* **195,** no. 3, 1773–1785, doi: 10.1093/gji/ggt331.

Eaton, D., M. van der Baan, J. B. Tary, B. Birkelo, N. Spriggs, S. Cutten, and K. Pike (2013). Broadband microseismic observations from a Montney hydraulic fracture treatment, northeastern BC, Canada, *CSEG Rec.* **38,** no. 3, 44–53.

Gerstoft, P., and T. Tanimoto (2007). A year of microseisms in southern California, *Geophys. Res. Lett.* **34,** L20304, doi: 10.1029/2007GL031091.

Hu, H., A. Li, and R. Zavala-Torres (2017). Long-period long-duration seismic events during hydraulic fracturing: Implications for tensile fracture development, *Geophys. Res. Lett.* **44,** no. 10, 4814–4819, doi: 10.1002/2017GL073582.

Kanamori, H., and E. Hauksson (1992). A slow earthquake in the Santa Maria basin, California, *Bull. Seismol. Soc. Am.* **82,** no. 5, 2087–2096.

Kao, H., and S. Shan (2004). The source-scanning algorithm: Mapping the distribution of seismic sources in time and space, *Geophys. J. Int.* **157,** no. 2, 589–594, doi: 10.1111/j.1365-246X.2004.02276.x.

Kohli, A. H., and M. D. Zoback (2013). Frictional properties of shale reservoir rocks, *J. Geophys. Res.* **118,** 5109–5125, doi: 10.1002/jgrb.50346.

Kumar, A., E. Zorn, R. Hammack, and W. Harbert (2017). Long-period, long-duration seismicity observed during hydraulic fracturing of the Marcellus Shale in Greene County, Pennsylvania, *The Leading Edge* **36,** no. 7, 580–587, doi: 10.1190/tle36070580.1.

Li, C., Z. Li, Z. Peng, and C. Zhang (2017). Detecting micro-seismicity and long-duration tremor-like events from the Oklahoma wavefield experiment, presented at the *2017 Fall Meeting, AGU*, New Orleans, Louisiana, 11–15 December, Abstract S41C–0797.

Liang, X., X. Liu, H. Shu, C. Xian, Z. Zhang, C. Zhao, Q. Li, and L. Zhang (2015). Characterization of complex multiscale natural fracture systems of the Silurian LongMaXi Gas Shale in the Sichuan Basin, China, paper presented at the *SPE Asia Pacific Unconventional Resources Conf. and Exhibition*, Brisbane, Australia, 9 November.

Tary, J. B., M. van der Bann, and D. W. Eaton (2014). Interpretation of resonance frequencies recorded during hydraulic fracturing treatments, *J. Geophys. Res.* **119,** 1295–1315, doi: 10.1002/2013JB010904.

Tary, J. B., M. van der Bann, B. Sutherland, and D. W. Eaton (2014). Characteristics of fluid-induced resonances observed during microseismic monitoring, *J. Geophys. Res.* **119,** no. 11, 8207–8222, doi: 10.1002/2014JB011263.

Wessel, P., W. H. F. Smith, R. Scharroo, J. F. Luis, and F. Wobbe (2013). Generic Mapping Tools: Improved version released, *Eos Trans. AGU* **94,** no. 45, 409–410, doi: 10.1002/2013EO450001.

Zecevic, M., G. Daniel, and D. Jurick (2016). On the nature of long-period long-duration seismic events detected during hydraulic fracturing, *Geophysics* **81,** no. 3, KS109–KS117, doi: 10.1190/GEO2015-0524.1.

Zoback, M. D., A. Kohli, I. Das, and M. McClure (2012). The importance of slow slip on faults during hydraulic fracturing stimulation of shale gas reservoirs, *Americas Unconventional Resources Conf.*, Pittsburgh, Pennsylvania, 5–7 June.

***Haichao Chen*[1]**
***Fenglin Niu*[2]**
Youcai Tang
Kai Tao
Unconventional Natural Gas Institute, and State Key Laboratory of Petroleum Resources and Prospecting
China University of Petroleum
No. 18 Fuxue Road, Changping District
Beijing 102249, China
chchao@cup.edu.cn
niu@cup.edu.cn
tangyc@cup.edu.cn
taokai@cup.edu.cn

Published Online 21 February 2018

[1] Also at Seismological Laboratory, California Institute of Technology, 1200 E. California Boulevard, MS 252-21, Pasadena, California 91125-2100 U.S.A.

[2] Also at Department of Earth, Environmental and Planetary Sciences, Rice University, 6100 Main Street, MS-126, Houston, Texas 77005 U.S.A.; niu@rice.edu.